SnO2-Based Hierarchical Nanomicrostructures: Facile Synthesis and Their Applications in Gas Sensors and Lithium-Ion Batteries

ARTICLE *in* THE JOURNAL OF PHYSICAL CHEMISTRY C · AUGUST 2009

Impact Factor: 4.77 · DOI: 10.1021/jp904209k

4 AUTHORS, INCLUDING:

Xing-Long Wu
Northeast Normal University
62 PUBLICATIONS **3,173** CITATIONS
SEE PROFILE

Yu-Guo Guo
Chinese Academy of Sciences
170 PUBLICATIONS **10,880** CITATIONS
SEE PROFILE

SnO_2-Based Hierarchical Nanomicrostructures: Facile Synthesis and Their Applications in Gas Sensors and Lithium-Ion Batteries

Ling-Yan Jiang,† Xing-Long Wu,† Yu-Guo Guo,* and Li-Jun Wan*

Key Laboratory of Molecular Nanostructure and Nanotechnology, Institute of Chemistry, Chinese Academy of Sciences (CAS), Beijing 100190, China and Beijing National Laboratory for Molecular Sciences (BNLMS), Beijing 100190, China

Received: May 6, 2009; Revised Manuscript Received: June 12, 2009

Hierarchical flower-like SnO_2 nanomicrostructure has been synthesized via a solvent-induced and surfactant assisted self-assembly technique at ambient temperature followed by a suitable thermal treatment. A possible growth mechanism governing the formation of such a nanomicrostructure is discussed. The applications in gas sensors for detecting CO and H_2 reveal that the obtained SnO_2 material exhibits a remarkable sensitivity and extremely low detecting limit (5 ppm), as well as good reproducibility and short response/recovery times, which benefit a lot from its unique flower-like nanomicrostructure consisting of three-dimensional interconnected SnO_2 nanoparticles and nanopores. In order to use the present SnO_2 nanomicrostructure in lithium-ion batteries, carbon coatings are introduced to the surface of them by pyrolysis of glucose under hydrothermal conditions. Both SnO_2−C and Sn−C nanocomposites are obtained by taking thermal treatment of the precursors at different temperatures. The conversion processes are investigated by thermogravimetrics (TG) analyses under N_2 and air atmosphere. All three Sn-based nanostructures are investigated with XRD, SEM, TEM, and electrochemical tests toward lithium storage. It is found that the SnO_2−C composite shows a very high reversible capacity (~700 mA h g^{-1} after 20 cycles) and high Coulombic efficiency in the initial few cycles, as well as significantly enhanced cycling performance compared with bare SnO_2 nanostructure and Sn−C nanocomposite, exhibiting great potential as an anode material in lithium-ion batteries. The improvements can be attributed to the outside carbon coating layer as well as the in situ formed buffer, Li_2O matrix, upon initial Li uptake.

1. Introduction

Tin oxide, a wide band gap n-type semiconductor, is of great importance essentially because of its wide range of applications: it is used as a catalyst, gas sensor, and anode material for lithium-ion batteries (LIBs).[1−6] Of great interests are nanostructured SnO_2, whose properties could be significantly improved compare with its bulk material benefiting from nanometer size effects.[7,8] Right promoted by this expectation, various nanostructures of SnO_2 and SnO_2-based composites such as nanoparticles, nanowires, nanorods, hollow nanostructures, and mesoporous solids have been synthesized.[9−12] These nanostructures have demonstrated very promising results for gas sensing and energy storage.[3−6,10,11,13−19] For example, Yan et al.[4] successfully prepared nanocrystalline porous SnO_2 by an ionic liquids assisted technique and evaluated its gas sensing properties, which reveal highly sensitive, fast-responding, reproducible, and size selective sensing behaviors. Liu et al.[6] explored the structural evolution of SnO_2 fine powder during lithium insertion and predicted the potential application for LIBs. Lou et al.[10,11] synthesized high-quality SnO_2 hollow nanostructures by using both template-free and templating strategies, which exhibit enhanced electrochemical activity toward lithium insertion. So far it has been demonstrated that the multiscale structure and morphology of functional nanomaterials has a remarkable effect on their sensing and electrochemical properties.[20−23] Fundamental advances in the designs, synthesis, and control of multiscale structure in advanced SnO_2 nano/micro hierarchical structures would lead to superior gas sensors and LIBs.

For achieving a high sensitivity of gas sensors, there has always been a need for developing active materials with large surface areas readily accessible to analyte molecules.[4,5] Flower-like nano/micro structure with open three-dimensional (3D) porous structure is one of the best systems of choice because it can take both the advantages of nanometer-sized building blocks and micrometer-sized flower-like assemblies.[24] While the former provides high surface areas and hence is the key to the high sensitivity, the latter guarantees favorable kinetics and fast-responding sensing behaviors. It has been reported that the transport of small molecules in flower-like media can approach rates of diffusion comparable to those in open medium, which make this kind of hierarchical structure an important issue to be addressed in the context of gas sensors as well as catalysts.[24] However, large-scale synthesis of well-defined flower-like SnO_2 nanomicrostructure is still a challenge. Herein, we report a reliable and facile solvent-induced and surfactant assisted self-assembly method to produce such a structure of tin(II) oxalate. By simply calcining the flower-like SnC_2O_4 precursor, highly porous flower-like SnO_2 nanomicrostructure consisting of interconnected SnO_2 nanoparticles was obtained. The applications in gas sensors for the SnO_2 nanomicrostructure exhibit highly sensitive and fast-responding sensing behaviors.

Tin-based materials have also been of considerable interest as promising anode materials for LIBs because of their higher Li storage capacity, which provides higher energy density than commercial Li-intercalated carbons. When SnO_2 is used as the anode material, both a conversion mechanism and an alloy mechanism are involved. The former is mainly related to in

* Corresponding author. E-mail: ygguo@iccas.ac.cn. Phone or Fax: (86)10-62557908.
† Also at the Graduate School of CAS, Beijing 100049, China.

10.1021/jp904209k CCC: $40.75
Published on Web 07/06/2009

situ formation of metal, here, the metallic Sn and Li_2O matrix nanocomposites upon the initial Li uptake like that which has been widely reported for transition metal oxides,[25] while the latter is the alloying process of Sn upon more Li uptake:

$$SnO_2 + 4Li^+ + 4e^- \rightarrow Sn + 2Li_2O \quad (1)$$

$$Sn + xLi^+ + xe^- \rightarrow Li_xSn \quad (0 \le x \le 4.4) \quad (2)$$

Usually, the alloying reaction 2 is thought to be highly reversible, giving a theoretical lithium storage capacity of 782 mA h g^{-1} ($Li_{4.4}Sn$). Reaction 1, which is usually reported to be irreversible, may also become reversible for nanostructured SnO_2[15] and hence could contribute an extra capacity of 711 mA h g^{-1}. The total capacity of SnO_2 is then calculated to be 1493 mA h g^{-1}, which is much higher than that of conventional graphite (Li_6C, 372 mA h g^{-1}). However, practical use of the high-capacity anode material is still largely hindered by the huge volume variation during Li uptake/release cycles, which leads to pulverization of the electrode and very rapid capacity decay.[26−28] It has been demonstrated that this problem can be partly solved in nanostructured SnO_2 and Sn-based composite materials because of better accommodation of the stains of Li uptake/release than in micrometer-scale SnO_2.[29−33] However, the high surface area of nanostructured electrode materials raises the risk of secondary reactions involving electrolyte decomposition between electrode and electrolyte, which causes a high level of irreversibility (i.e., low columbic efficiency) and poor cycle life, and the formation of thick solid electrolyte interphase (SEI) layers on the electrode surface, which consume much of the Li supplied by the cathodes.[34] Carbon coating may be an effective way to improve the cycling performance as well as the initial Coulombic efficiency based on the hypothesis that the inherent stable carbon shell not only plays an important role as structural buffering layer to mitigate the mechanical stress caused by large volume change but also leads to relatively stable SEI layers on its surface.[35−37] From this point of view, carbon-coated SnO_2 nanostructures should be desirable for superior electrode performance. In the present work, we therefore introduced carbon coatings on the surface of flower-like SnO_2 nanomicrostructures. Nanostructured SnO_2−C and Sn−C composites have been successfully synthesized by using different thermal treatments. Significantly enhanced electrochemical performance toward Li storage is found in the SnO_2−C composite in terms of reversible capacity, Coulombic efficiency, and cycling performance compared with bare SnO_2 nanomicrostructures and Sn−C composite, exhibiting great potential as anode materials in LIBs.

2. Experimental Section

2.1. Preparation of Flower-Like SnO_2 Nanomicrostructures. All of the reagents were received from Beijing Chemicals Co. (Beijing, China) and used without further purification. In a typical synthesis, 1.46 g of $H_2C_2O_4$ was dispersed into a mixed solution containing 120 mL of ethanol and 40 mL of polyethylene glycol (PEG-600) under stirring. Then, 1.78 g of $SnCl_2 \cdot 2H_2O$ was introduced into the solution when the $H_2C_2O_4$ was dissolved completely, followed by dropwise adding 16 mL of deionized (DI) water. After stirring for several minutes, the as-prepared precipitate was separated by centrifugation and washed with distilled water and ethanol for several times. The dried products were annealed at 500 °C under air for 2 h to obtain the flower-like SnO_2 nanomicrostructures.

2.2. Preparation of Carbon Coated Nanomicrostructures. 150 mg of SnO_2 was added to 4 mL of DI water to create a suspension. 800 mg of glucose and 10 mL of ethanol was put into 16 mL of DI water to obtain a transparent solution. The mixture of the above suspension and solution was transferred and sealed into a 40 mL Teflon-lined autoclave, then heated at 180 °C for 16 h. The dark precipitate was collected and washed with DI water. The products were heated in a quartz tube at 600 and 750 °C for 3 h, respectively, for preparing the SnO_2−C and Sn−C composites.

2.3. Characterization. X-ray powder diffraction (XRD) analysis was performed with a Rigaku D/max-2500 using filtered Cu Kα radiation. A JEOL model 2010F transmission electron microscope (TEM, operating at 200 kV) and a JEOL model 6701F field-emission scanning electron microscope (SEM, operating at 10 kV) were used to investigate the morphology and size of the as-obtained products. Thermogravimetrics (TG) analysis was carried out using a Perkin-Elmer model Pyris 1 thermal analysis equipment.

2.4. Electrochemical Characterization. Electrochemical measurements were performed using two-electrode Swagelok-type cells assembled in an argon-filled glovebox. For preparing working electrodes, a mixture of the active materials, acetylene black, and poly(vinyl difluoride) (PVDF) at a weight ratio of 80:10:10 was pasted on a Cu foil. A glass fiber (GF/D) from Whatman was used as a separator. Lithium foil was used as the counter electrode. The electrolyte consisted of a solution of 1 M $LiPF_6$ in ethylene carbonate (EC)/dimethyl carbonate (DMC)/diethyl carbonate (DEC) (1:1:1 in wt %) obtained from Novolyte Technologies (Suzhou) Co., Ltd. A galvanostatic cycling test of the assembled cells was carried out on an Arbin BT2000 system in the voltage range of 0.02−3.0 V or 0.02−2.2 V (vs Li^+/Li) at a discharge/charge rate of C/5.

2.5. Gas-Sensing Characterization. Gas-sensing measurements were performed using a homemade system.[38] Sensitive materials were dispersed in ethanol and dropped to UST microheat plate devices to form sensitive layers. Mass flow controllers (MFCs) were used to control a wide rage of concentration gas flow with a constant total rate of 200 sccm including synthetic air and the target gas (H_2 or CO). The sensor devices were heated by an Agilent E3640A programmable DC power supply, and the resistances of the sensitive layers were acquired by a Keithley 2400 source meter. All experiments were carried out at 320 °C after a warm-up process at the same temperature for about an hour.

3. Results and Discussion

3.1. Characterization of SnO_2 Precursor. The morphology of as-synthesized precursor was studied by SEM. Figure 1a shows the SEM image of a typical sample composed of many flower-like nanomicrostructures approximately 6 μm in diameter, which are built from several fanlike nanopetals. These nanopetals were self-assembled from nanorods and connected to each other through the center to form 3D flower-like structures. The composition and crystal structure of the as-obtained samples were determined by XRD. Figure 1b shows the XRD pattern of the flower-like precursor in which all diffraction peaks are in good agreement with monoclinic tin oxalate (JCPDS Card No. 51−0614). No other peaks are observed, indicating the high purity of the as-prepared SnC_2O_4 precursor.

In order to understand the formation process of the flower-like SnC_2O_4 precursor, we carried out detailed experiments during which samples were collected at different synthesis steps and time intervals. As shown in Figure 2a, the precipitate

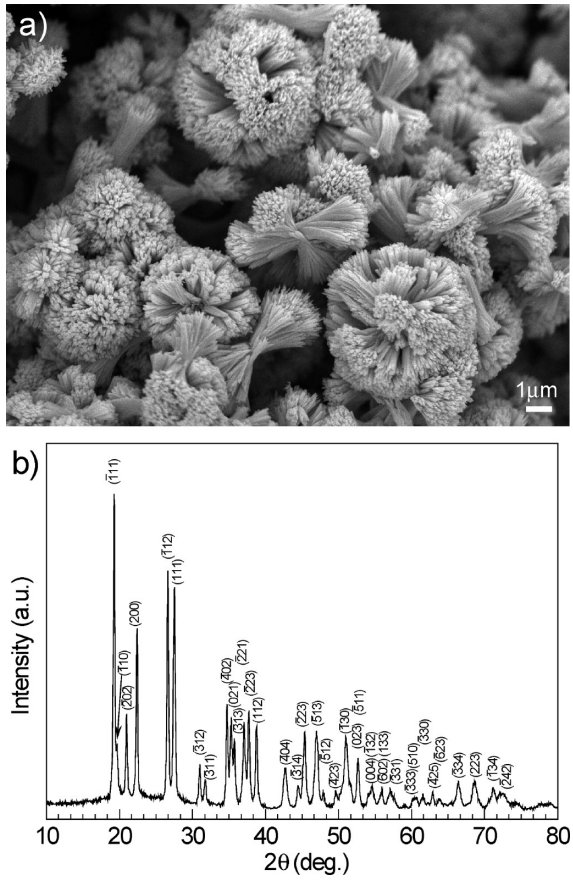

Figure 1. (a) SEM image and (b) XRD pattern of the as-prepared flower-like precursor.

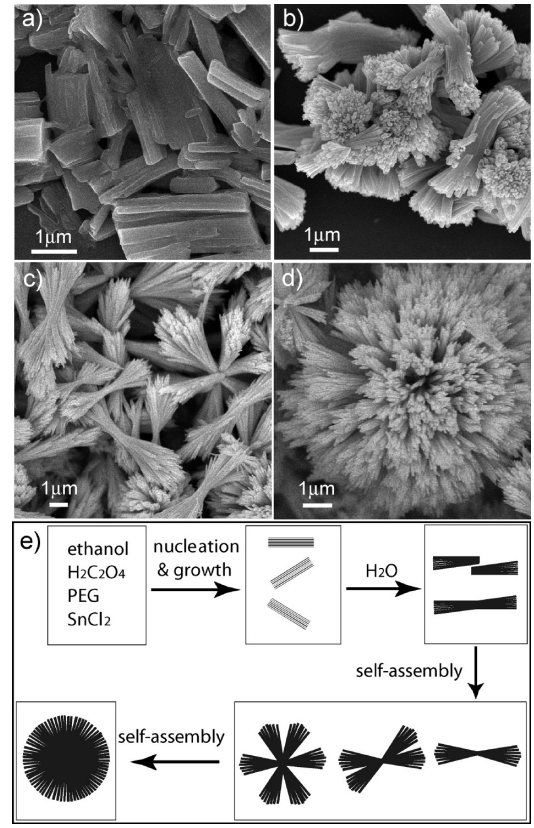

Figure 2. SEM images of the SnC_2O_4 precursors collected at different synthesis steps and time intervals: (a) before adding DI water, (b) 2 min, (c) 30 min, and (d) 60 min after adding DI water. (e) Schematic illustration of the morphological evolution process of the precursor.

appeared in the ethanol solution containing $H_2C_2O_4$ and $SnCl_2$ and PEG was in the shape of bundle composed of many nanorods. After the dropwise adding of DI water, at the early stage, the nanorod bundles became loose and divergent at the heads in the existence of PEG surfactant (Figure 2b). Two bundles tended to form a "dimer" in end-to-end fashion. The sample collected 30 min later (Figure 2c) showed many "diamers" with more divergent heads just forming the fanlike nanopetals. As the reaction proceeded, the number of nanopetals in certain assembles increased and finally resulted in the formation of 3D flower-like nanomicrostructures, as shown in Figure 2d.

The whole evolution process is illustrated in Figure 2e. In this formation process, PEG and H_2O were found to be the two key controlling factors. While the former could coordinate with $SnCl_2$ to produce tin alkoxide and accounts for the formation of nanorod like building blocks, which is similar to the function of EG in many EG-mediated process,[12,39] the latter, as a poor solvent for SnC_2O_4, might promote the exchange between $C_2O_4^{2-}$ and alkoxide as well as the self-assembly with the help from PEG surfactant. Other factors, including crystal-face attraction of $Sn_2C_2O_4$, hydrophobic interactions may also have effects on the self-assembly process. Further work is underway to investigate the detail of the self-assembly growth mechanism.

3.2. Characterization of SnO_2 Nanomicrostructure. Thermal treatment of metal oxalates was a simple route toward the synthesis of metal oxides.[40] The flower-like SnC_2O_4 precursor was calcined at 500 °C in air for 2 h to obtain flower-like SnO_2 nanomicrostructures. Figure 3a shows the XRD pattern of the as-synthesized sample. All of the diffraction peaks in the pattern are in good agreement with tetragonal rutile SnO_2 (JCPDS No. 41−1445, S.G.:$P4_2/mnm$, $a0 = b0 = 4.738$ Å, $c0 = 3.187$ Å), which confirms that pure SnO_2 could be obtained by this facile route.

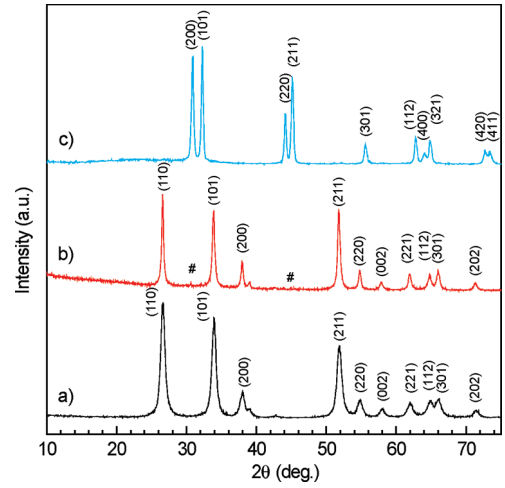

Figure 3. XRD patterns of (a) the flower-like SnO_2 nanomicrostructure, (b) SnO_2−C composite, (c) Sn−C composite. The small peaks marked (#) in (b) belong to orthorhombic SnO (JCPDS No. 24−1342).

Calcination did not change the flower-like morphology of the SnC_2O_4 precursor, as shown by Figure 4a. However, SEM image at high magnification (Figure 4b) revealed that, after calcination, each nanorod of the flower-like structure had been transformed from a dense structure with a smooth surface into a highly porous structure consisting of interconnected nanoparticles, because of the removal of organic species in the precursor during annealing. The size of these nanoparticles ranged between 20

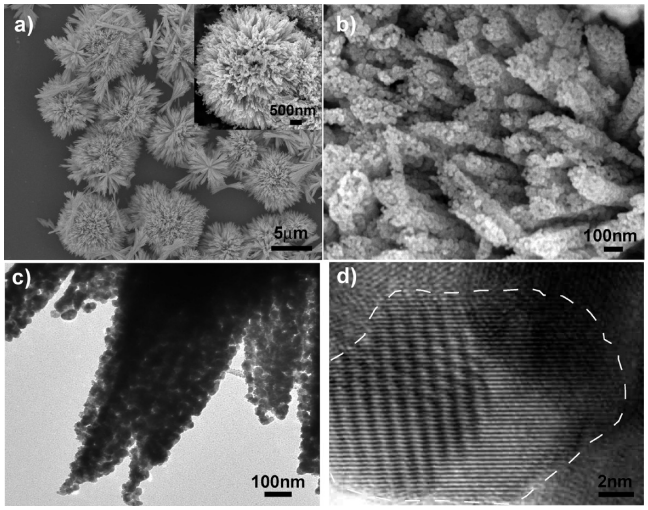

Figure 4. (a,b) SEM, (c) TEM, and (d) HRTEM images of the as-obtained flower-like SnO_2 nanomicrostructures. The inset in (a) is a close view of a single flower-like structure.

and 30 nm, which was also confirmed by TEM observation (Figure 4c). A representative high-resolution TEM (HRTEM) image taken from the SnO_2 nanoparticle is shown in Figure 4d indicated by dash line. The lattice fringes are clearly visible with a spacing of 0.24 nm, corresponding to the spacing of the (200) planes of tetragonal rutile SnO_2. The Brunauer−Emmett−Teller (BET) gas sorptometry measurement showed that the flower-like SnO_2 has a specific surface area of ~25 m^2 g^{-1}.

3.3. Gas-Sensing Properties of Flower-Like SnO_2 Nanomicrostructure. Tin dioxide is one of the most popular semiconducting oxides for sensor. The hierarchical nanomicrostructure of SnO_2 is expected to enhance its sensing performance for gas. Figure 5 presents the results for H_2 and CO sensing obtained from the flower-like SnO_2 nanomicrostructure. It is obvious that the sensor showed remarkably high sensitivity and reversibility. The gradual augmentation of sensitivity can be observed with the increase of the gas concentration (Figure 5b,d). The detection limit for both H_2 and CO can be as low as 5 ppm. As far as SnO_2-based sensors are concerned, it is one of the best sensing performances ever measured.[4] The response and recovery times (time to reach 90% of the total resistance variation) for H_2 were only 20 s and 35 s, respectively, suggesting that the sensors respond quickly to both the introduction and the removal of small amounts of target gases in air (Figure 5c). Furthermore, the reversibility and stability are

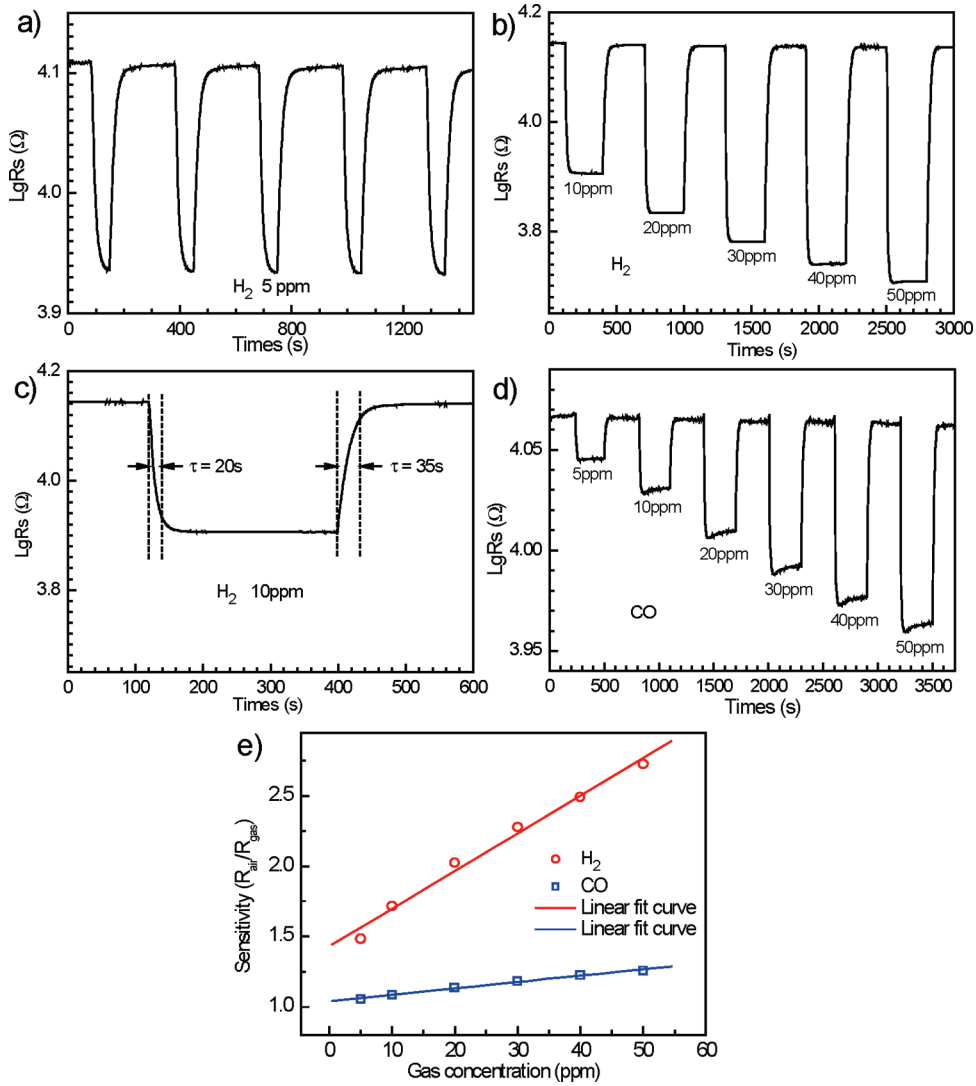

Figure 5. (a) Gas-sensing behavior of the flower-like SnO_2 nanomicrostructure for H_2. (b) Variation of the sensor response with the change of the concentration of H_2. (c) The response and recovery times for H_2 at 10 ppm. (d) Variation of the sensor response with the change of the concentration of CO. (e) Linear dependence relation between resistance response sensitivity and gas concentration.

demonstrated by the complete recovery of the air resistance value after switching off the target gas during many cycles, which suggests the highly reversible interactions between the analytes and the sensor elements. We also note that the response sensitivity (R_{air}/R_{gas}) of the flower-like SnO_2 nanomicrostructure-based sensor presents a good linearity with the concentration of target gas (Figure 5e). The sensitivity of the sensor toward H_2 is much larger than that to CO in the concentration range of 5−50 ppm (Figure 5e). The results indicate that the flower-like SnO_2 nanomicrostructure-based sensor has high selectivity to smaller H_2 molecules. Such differences in the sensing behaviors may be related to the effects of steric hindrance on the diffusion and accessibility of the target gases to the deeper region of the SnO_2 layers in view of the different molecular sizes of H_2 and CO.

For SnO_2-based sensors, the sensing mechanism is mainly due to the surface conductivity modulation by the adsorption and desorption of gas molecules.[12] Therefore, the diffusion of gas molecules across the surface of the sensing structure affects the sensitivity remarkably.[41,42] For the SnO_2 sensor described here, we believe that the high sensing performance can be attributed to the novel hierarchical nanomicrostructure. On one hand, the flower-like microstructures result in the formation of two 3D networks, one consisting of interconnected SnO_2 nanoparticles and the other consisting of interconnected nanopores. While the former can improve interconnection of nanosized components and hence shorten the transfer of electrons or signals, the latter is favorable for the target gas transportation and accessibility.[43] On the other hand, the nanosized SnO_2 nanoparticles provide a large contact area between sensing materials and sensing species and thus is the key to the much enhanced sensitivity and lowered detecting limit.[44]

3.4. Characterization of SnO_2−C and Sn−C Nanocomposite. Carbon coating is one of the most widely used techniques for improving the electrochemical performance of electrode materials because carbon coating layers can enhance the electronic conductivity of electrode materials, lead to the formation of relatively stable SEI films on their surfaces, and encompass better accommodation of the strain of Li^+ insertion/extraction.[3,33,37] In order to use the present flower-like SnO_2 nanomicrostructures in LIBs, carbon coatings were introduced on the surface of them by pyrolysis of glucose under hydrothermal conditions.[37,45] Figure 6a−d shows the SEM and TEM images of as-obtained nanocomposites synthesized by heat-treatment of carbon-precursor-coated SnO_2 at 600 and 750 °C for 3 h, respectively. Both of the two nanocomposites are no longer flower-like but nanomicrospheres with smooth surfaces and interconnected nanoparticles. The existence of carbon coating layers can be clearly seen from the TEM images (Figure 6b,d).

To clarify the structure of the composites, XRD experiments were carried out (Figure 3). It can be seen that the XRD pattern (Figure 3b) of the sample annealed at 600 °C is the same as that (Figure 3a) of the tetragonal rutile SnO_2 nanomicrostructure before carbon coating, except for two small peaks marked by #, which are corresponding to orthorhombic SnO (JCPDS No. 24−1342). Figure 3c shows XRD pattern of the sample annealed at 750 °C in which all diffraction peaks can be well-indexed to tetragonal Sn (JCPDS No.04−0673, S.G.:$P4_1/amd$, $a0 = b0 = 5.831$ Å, $c0 = 3.182$ Å). The existence of metallic Sn is also confirmed by the HRTEM image (Figure 6d) taken from a nanoparticle of the composite shown in Figure 6c. The lattice fringes are clearly visible with a spacing of 0.29 nm, corresponding to the spacing of the (200) planes of tetragonal Sn (see inset in Figure 6d). The results confirm that both SnO_2−C composite and Sn−C composite could be obtained by this facile

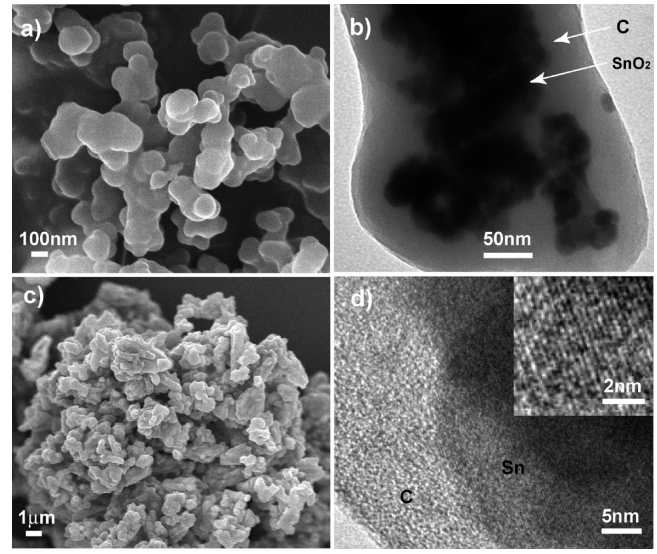

Figure 6. (a) SEM and (b) TEM images of the obtained SnO_2−C nanocomposite. (c) SEM and (d) TEM images of the obtained Sn−C nanocomposite. The inset in (d) is a HRTEM image taken from the Sn part.

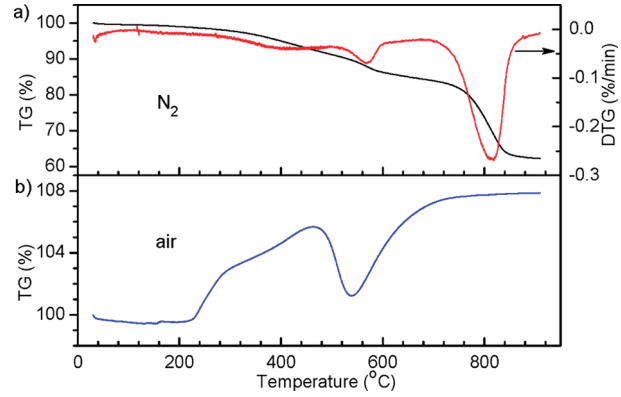

Figure 7. TG results of (a) carbon precursor coated SnO_2 nanostructure under N_2 atmosphere, and (b) as-obtained Sn−C nanocomposite under air atmosphere.

route. Note that no obvious XRD peaks corresponding to graphite are found in the two XRD patterns of SnO_2−C and Sn−C composites (Figure 3b,c), which indicate the carbon coatings in the two composites are not well-crystallized.

Thermogravimetrics (TG) analyses were carried out to investigate the conversion process from carbon precursor coated SnO_2 nanomicrostructures into SnO_2−C and Sn−C composites as well as the chemical compositions of the two composites. Figure 7a shows the TG result of dried SnO_2−carbon precursor under N_2 atmosphere. There are three obvious weight loss valleys in the corresponding DTG curve above 100 °C. The one at 400 °C relates to the carbonization of carbon precursor, while the other two can be attributed to the following chemical reactions between SnO_2 and carbon:

$$2SnO_2 + C \rightarrow 2SnO + CO_2 \quad (3)$$

$$2SnO + C \rightarrow 2Sn + CO_2 \quad (4)$$

$$SnO_2 + C \rightarrow Sn + CO_2 \quad (5)$$

First, SnO_2 partially reacts with bordering carbon shells to produce SnO at about 570 °C, as confirmed by XRD. Then,

the as-formed SnO and SnO_2 further react with excessive carbon between 700 and 880 °C, leading to the formation of metallic Sn. Therefore, the sample annealed at 600 °C is mainly SnO_2−C composite, while that annealed at 750 °C is Sn−C composite. Figure 7b represents TG result of the Sn−C composite under air atmosphere. The mass of the sample stays almost unchanged below 200 °C, which indicates that the sample is quite stable under ambient atmosphere. When the temperature rises, the following reactions occur:

$$C + O_2 \rightarrow CO_2 \quad (6)$$

$$2Sn + O_2 \rightarrow 2SnO \quad (7)$$

$$2SnO + O_2 \rightarrow 2SnO_2 \quad (8)$$

$$Sn + O_2 \rightarrow SnO_2 \quad (9)$$

Reaction 6 results in a mass decrease, while reactions 7−9 lead to an increase of mass. After the temperature rises to 900 °C, all carbon and tin in the composite have converted to CO_2 and SnO_2, respectively, according to the reactions 6 and 9. The overall mass change is a gain of 7.78 wt % as indicated in the TG curve (Figure 7c). It can be accordingly calculated that the Sn−C and the SnO_2−C composites contain 91 wt % Sn and 9 wt % C, and 86 wt % SnO_2 and 14 wt % C, respectively.

3.5. Electrochemical Performance toward Lithium Storage. To investigate the carbon coating effects on the electrochemical properties of the three Sn-based nanostructures, we carried out a preliminary investigation into their electrochemical performance with respect to Li insertion/extraction. Figure 8 shows the first and the second discharge/charge voltage profiles for the SnO_2, SnO_2−C, and Sn−C nanostructures at a rate of *C*/5 between the voltage limits of 0.02 and 3.0 V (vs Li^+/Li). With regard to the first cycle, it is found that both the SnO_2 and the SnO_2−C nanostructures have a long plateau at around 0.9 V, which can be ascribed to the "conversion" lithium storage mechanism (see eq 1) and is quite similar to that reported for nanostructured SnO_2.[15] Though the SnO_2 nanostructure before and after carbon coating show a very close discharge capacity (ca. 1782 and 1626 mA h g^{-1}, respectively), the SnO_2−C composite has a much higher charge capacity (ca. 1209 mA h g^{-1}) when compared with the SnO_2 without carbon coating layer (ca. 817 mA h g^{-1}). The results indicate that the SnO_2−C composite exhibits an initial Coulombic efficiency of about 74% (Figure 9b), which is remarkably higher than that of the SnO_2 nanostructure (46%) and other reports.[14,15] The improvement of initial Coulombic efficiency can be attributed to the carbon coating layer as has been reported in many carbon-coated materials.[37] On one hand, carbon materials are very stable anode materials in LIBs because of the small volume change during Li insertion/extraction. On the other hand, the SEI films on carbon surface are also relatively stable compared with transition metal oxides.

As for the Sn−C composite (Figure 8c), several plateaus between 0.4 and 0.8 V are observed in the first discharge curve implying the well-known multistep Sn−Li alloying process.[15,29,33] Interestingly, an extremely high initial Coulombic efficiency of 97% was obtained because of the existence of two more charge plateaus above 2.8 V in the first charge curve (Figure 8c). The two plateaus disappear in the subsequent cycles. These phenomena have been discussed in detail in the literature[46] and can

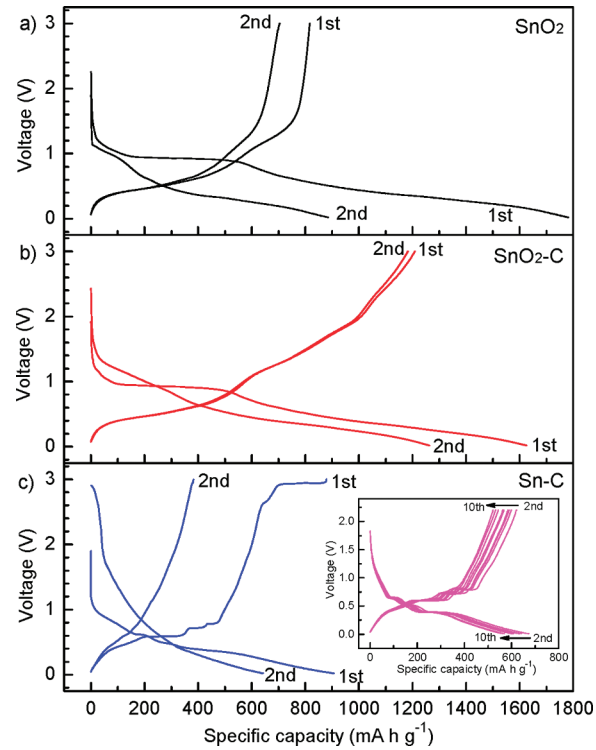

Figure 8. First and the second discharge/charge profiles for the (a) SnO_2, (b) SnO_2−C, and (c) Sn−C samples cycled at a rate of *C*/5 between the voltage limits of 0.02 and 3.0 V (vs Li^+/Li). The inset in (c) is the discharge/charge profiles for the Sn−C sample cycled at the same rate but between the voltage limits of 0.02 and 2.2 V (vs Li^+/Li).

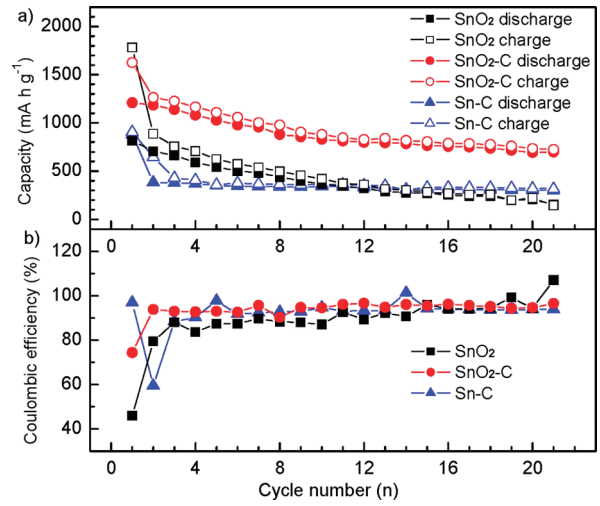

Figure 9. (a) Cycling performance and (b) corresponding coulombic efficiency profiles of the SnO_2, SnO_2−C, and Sn−C samples at a rate of *C*/5 between voltage limits of 0.02 and 3.0 V.

be attributed mainly to the decomposition of $ROCO_2Li$ in SEI layer induced by nanosized tin particles. When the voltage was limited between 0.02 and 2.2 V, the Sn−C nanocomposite exhibits much better cycling performance with a reversible capacity of around 550 mA h g^{-1}, as shown in the inset of Figure 8c.

Figure 9 shows the cycling performance and corresponding Coulombic efficiency profiles of the SnO_2, SnO_2−C, and Sn−C samples at a rate of *C*/5 between voltage limits of 0.02 and 3.0 V. It is clearly seen that the SnO_2−C composite exhibits the best cycling performance among the three Sn-based nanostructures. After 20 cycles, the reversible capacity for SnO_2−C

composite is still as high as 700 mA h g^{-1}, while that for SnO_2 nanostructure and Sn−C composite is only 200 and 300 mA h g^{-1}, respectively. It is much higher than the theoretical specific capacity of currently used graphite (LiC_6, 372 mA h g^{-1}) and makes the SnO_2−C composite a promising anode material for LIBs.

The above-mentioned superior electrochemical performance of SnO_2−C nanocomposite as anode materials for LIBs could be attributed to the following two factors. First, the carbon coating layer can maintain the integrity of active particles, lead to a stabilized surface toward the formation of SEI films, and therefore enhance the initial Coulombic efficiency, specific capacity, and cycling performance of electrode materials as has been reported in many transition metal oxides.[37] The robustness of the carbon layer of the SnO_2−C composite was confirmed by our TEM observation of the postused sample (see Figures S1 in Supporting Information). Second, the Li_2O matrix in situ formed upon the initial Li uptake also is helpful for maintaining the high capacity, because it can act as a buffer for relieving the strain associated with the volume variations during Li−Sn alloying−dealloying processes.[12,47]

4. Conclusions

In summary, a hierarchical flower-like SnO_2 nanomicrostructure was synthesized by a facile solvent-induced and surfactant assisted self-assembly method followed by a suitable thermal treatment. After introducing carbon coating layers, both SnO_2−C and Sn−C nanocomposites were obtained by taking thermal treatment at different temperatures. The SnO_2 nanostructure exhibits high sensitivities toward CO and H_2, an extremely low detecting limit (5 ppm), and remarkably short response/recovery times (ca. 20 s/35 s). Electrochemical measurements show that the SnO_2−C composite has the best electrochemical performance toward lithium storage in terms of specific capacity, Coulombic efficiency, and cycling behavior. While the former is attributed to its unique flower-like nanomicrostructure with 3D interconnected SnO_2 nanoparticles and nanopores, and hence is the key to the high sensing performance, the latter is benefit from the outside carbon coating layer as well as the in situ formed matrix of Li_2O during Li uptake, both of which are good for maintaining a robust and stable lithium storage system. The results here not only provide further examples of the advantages of hierarchically nanomicrostructured materials in the fields of gas sensing, but also give clear evidence of the utility of carbon coatings in improving electrochemical performance of nanostructured electrode materials for LIBs.

Acknowledgment. This work is supported by the National Natural Science Foundation of China (NSFC Nos. 50730005 and 20701038), Ministry of Science and Technology (MOST Nos. 2006CB806100 and 2009CB930400), and the Chinese Academy of Sciences.

Supporting Information Available: TEM image of the postused SnO_2−C composite in lithium batteries. This information is available free of charge via the Internet at http://pubs.acs.org.

References and Notes

(1) Brousse, T.; Retoux, R.; Herterich, U.; Schleich, D. M. *J. Electrochem. Soc.* **1998**, *145*, 1–4.
(2) Read, J.; Foster, D.; Wolfenstine, J.; Behl, W. *J. Power Sources* **2001**, *96*, 277–281.
(3) Derrien, G.; Hassoun, J.; Panero, S.; Scrosati, B. *Adv. Mater.* **2007**, *19*, 2336–2340.
(4) Li, L.-L.; Zhang, W.-M.; Yuan, Q.; Li, Z.-X.; Fang, C.-J.; Sun, L.-D.; Wan, L.-J.; Yan, C.-H. *Cryst. Growth Des.* **2008**, *8*, 4165–4172.
(5) Xu, G.; Zhang, Y.-W.; Sun, X.; Xu, C.-L.; Yan, C.-H. *J. Phys. Chem. B* **2005**, *109*, 3269–3278.
(6) Liu, W. F.; Huang, X. J.; Wang, Z. X.; Li, H.; Chen, L. Q. *J. Electrochem. Soc.* **1998**, *145*, 59–62.
(7) Wang, Y.; Cao, G. *Adv. Mater.* **2008**, *20*, 2251–2269.
(8) Maier, J. *Nat. Mater.* **2005**, *4*, 805–815.
(9) Deng, D.; Lee, J. Y. *Chem. Mater.* **2008**, *20*, 1841–1846.
(10) Lou, X. W.; Deng, D.; Lee, J. Y.; Archer, L. A. *Chem. Mater.* **2008**, *20*, 6562–6566.
(11) Lou, X. W.; Wang, Y.; Yuan, C. L.; Lee, J. Y.; Archer, L. A. *Adv. Mater.* **2006**, *18*, 2325–2329.
(12) Wang, Y.; Jiang, X.; Xia, Y. *J. Am. Chem. Soc.* **2003**, *125*, 16176–16177.
(13) Kuang, Q.; Lao, C.; Wang, Z. L.; Xie, Z.; Zheng, L. *J. Am. Chem. Soc.* **2007**, *129*, 6070–6071.
(14) Park, M.-S.; Wang, G.-X.; Kang, Y.-M.; Wexler, D.; Dou, S.-X.; Liu, H.-K. *Angew. Chem., Int. Ed.* **2007**, *46*, 750–753.
(15) Demir-Cakan, R.; Hu, Y.-S.; Antonietti, M.; Maier, J.; Titirici, M.-M. *Chem. Mater.* **2008**, *20*, 1227–1229.
(16) Kim, H.; Cho, J. *J. Mater. Chem.* **2008**, *18*, 771–775.
(17) Maranchi, J. P.; Hepp, A. F.; Kumta, P. N. *Mater. Sci. Eng., B* **2005**, *116*, 327–340.
(18) Wen, Z. H.; Wang, Q.; Zhang, Q.; Li, J. H. *Adv. Funct. Mater.* **2007**, *17*, 2772–2778.
(19) Yong Wang, J. Y. L. *Angew. Chem., Int. Ed.* **2006**, *45*, 7039–7042.
(20) Liang, H. P.; Lawrence, N. S.; Wan, L. J.; Jiang, L.; Song, W. G.; Jones, T. G. J. *J. Phys. Chem. C* **2008**, *112*, 338–344.
(21) Liang, H. P.; Lawrence, N. S.; Jones, T. G. J.; Banks, C. E.; Ducati, C. *J. Am. Chem. Soc.* **2007**, *129*, 6068.
(22) Liu, J.; Cao, G.; Yang, Z.; Wang, D.; Dubois, D.; Zhou, X.; Graff, G. L.; Pederson, L. R.; Zhang, J.-G. *ChemSusChem* **2008**, *1*, 676–697.
(23) Subramanian, V.; Zhu, H.; Wei, B. *J. Phys. Chem. B* **2006**, *110*, 7178–7183.
(24) Sun, C. W.; Sun, J.; Xiao, G. L.; Zhang, H. R.; Qiu, X. P.; Li, H.; Chen, L. Q. *J. Phys. Chem. B* **2006**, *110*, 13445–13452.
(25) Poizot, P.; Laruelle, S.; Grugeon, S.; Dupont, L.; Tarascon, J. M. *Nature* **2000**, *407*, 496–499.
(26) Kim, C.; Noh, M.; Choi, M.; Cho, J.; Park, B. *Chem. Mater.* **2005**, *17*, 3297–3301.
(27) Li, H.; Shi, L. H.; Lu, W.; Huang, X. J.; Chen, L. Q. *J. Electrochem. Soc.* **2001**, *148*, A915−A922.
(28) Courtney, I. A.; McKinnon, W. R.; Dahn, J. R. *J. Electrochem. Soc.* **1999**, *146*, 59–68.
(29) Li, H.; Shi, L.; Wang, Q.; Chen, L.; Huang, X. *Solid State Ionics* **2002**, *148*, 247–258.
(30) Sivashanmugam, A.; Kumar, T. P.; Renganathan, N. G.; Gopukumar, S.; Wohlfahrt-Mehrens, M.; Garche, J. *J. Power Sources* **2005**, *144*, 197–203.
(31) Hassoun, J.; Derrien, G.; Panero, S.; Scrosati, B. *Adv. Mater.* **2008**, *20*, 3169–3175.
(32) Qiao, H.; Zheng, Z.; Zhang, L. Z.; Xiao, L. F. *J. Mater. Chem.* **2008**, *43*, 2778–2784.
(33) Zhang, W. M.; Hu, J. S.; Guo, Y. G.; Zheng, S. F.; Zhong, L. S.; Song, W. G.; Wan, L. J. *Adv. Mater.* **2008**, *20*, 1160–1165.
(34) Guo, Y. G.; Hu, J. S.; Wan, L. J. *Adv. Mater.* **2008**, *20*, 2878–2887.
(35) Lee, K. T.; Jung, Y. S.; Oh, S. M. *J. Am. Chem. Soc.* **2003**, *125*, 5652–5653.
(36) Park, M.-S.; Kang, Y.-M.; Kim, J.-H.; Wang, G.-X.; Dou, S.-X.; Liu, H.-K. *Carbon* **2008**, *46*, 35–40.
(37) Zhang, W. M.; Wu, X. L.; Hu, J. S.; Guo, Y. G.; Wan, L. J. *Adv. Funct. Mater.* **2008**, *18*, 3941–3946.
(38) Zhang, W. M.; Hu, J. S.; Song, W. G.; Wan, L. J. *Sens. Actuators, B* **2007**, *123*, 454–460.
(39) Cao, A. M.; Monnell, J. D.; Matranga, C.; Wu, J. M.; Cao, L. L.; Gao, D. *J. Phys. Chem. C* **2007**, *111*, 18624–18628.
(40) Sun, H.; Kang, S.-Z.; Mu, J. *Mater. Lett.* **2007**, *61*, 4121–4123.
(41) Geng, B.; Zhan, F.; Jiang, H.; Xing, Z.; Fang, C. *Cryst. Growth Des.* **2008**, *8*, 3497–3500.
(42) Santacruz, I.; Nieto, M. I.; Moreno, R.; Faraldos, M.; Sastre, E. *Adv. Eng. Mater* **2005**, *7*, 858–861.
(43) Karkamkar, A. J.; Kim, S. S.; Mahanti, S. D.; Pinnavaia, T. *Adv. Funct. Mater.* **2004**, *14*, 507–512.
(44) Walcarius, A.; Mandler, D.; Cox, J. A.; Collinson, M.; Lev, O. *J. Mater. Chem.* **2005**, *15*, 3663–3689.
(45) Sun, X. M.; Li, Y. D. *Angew. Chem., Int. Ed.* **2004**, *43*, 597–601.
(46) Guo, B. K.; Shu, J.; Tang, K.; Bai, Y.; Wang, Z. X.; Chen, L. Q. *J. Power Sources* **2008**, *177*, 205–210.
(47) Kim, J. Y.; King, D. E.; Kumta, P. N.; Blomgren, G. E. *J. Electrochem. Soc.* **2000**, *147*, 4411–4420.

JP904209K

Supporting information for

SnO_2-Based Hierarchical Nanomicrostructures: Facile Synthesis and Their Applications in Gas Sensors and Lithium-Ion Batteries

Ling-Yan Jiang,[†] Xing-Long Wu,[†] Yu-Guo Guo, and Li-Jun Wan*

Key Laboratory of Molecular Nanostructure and Nanotechnology, Institute of Chemistry, Chinese Academy of Sciences (CAS), Beijing 100190, China.

Beijing National Laboratory for Molecular Sciences (BNLMS), Beijing 100190, China

[†] Also at the Graduate School of CAS, Beijing 100049, China

[*] Corresponding author. E-mail: ygguo@iccas.ac.cn, Tel. & Fax: (86)10-62557908

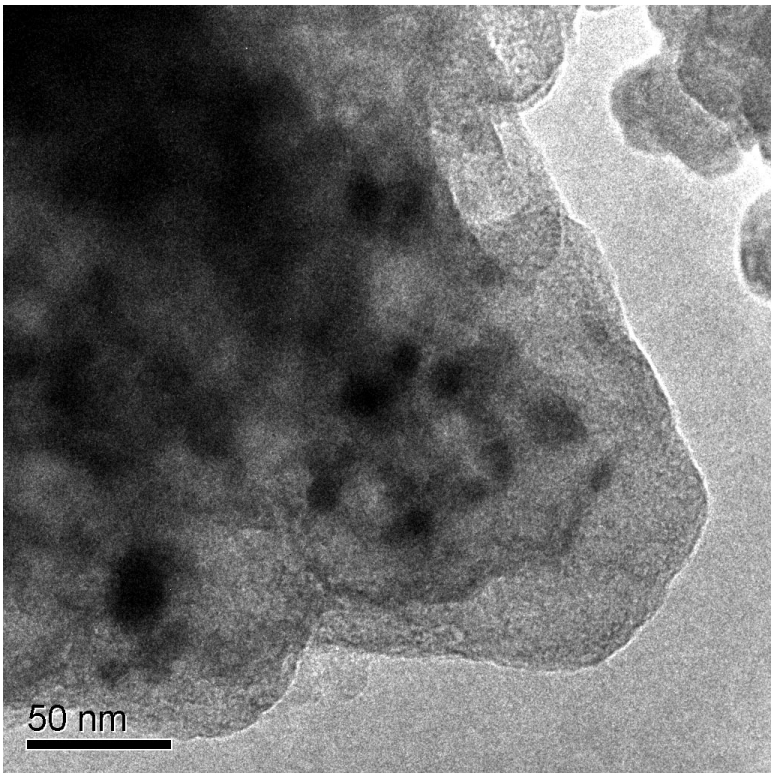

Figure S1. TEM image of the post-used SnO_2-C composite after four discharge/charge cycles at a rate of C/5 between the voltage limits of 0.02 – 3.0V.